Locating hydrothermal fluid injection of the 2018 phreatic eruption at Kusatsu-Shirane volcano with volcanic tremor amplitude

Taishi Yamada (yamada.taishi.8m@kyoto-u.ac.jp)
Kyoto University https://orcid.org/0000-0002-5919-9195
Aika K Kurokawa
National Research Institute for Earth Science and Disaster Resilience
Akihiko Terada
Volcanic Fluid Research Center, School of Science, Tokyo Institute of Technology
Wataru Kanda
Volcanic Fluid Research Center, School of Science, Tokyo Institute of Technology
Hideki Ueda
National Research Institute for Earth Science and Disaster Resilience
Hiroshi Aoyama
Institute of Seismology and Volcanology, Faculty of Science, Hokkaido University
Takahiro Ohkura
Aso Volcanological Laboratory, Kyoto University
Yasuo Ogawa
Volcanic Fluid Research Center, School of Science, Tokyo Institute of Technology
Toshikazu Tanada
National Research Institute for Earth Science and Disaster Resilience

Full paper

Keywords: Kusatsu-Shirane, Phreatic eruptions, Volcanic tremor, Hydrothermal system

Posted Date: September 16th, 2020

DOI: https://doi.org/10.21203/rs.3.rs-74868/v1

Version of Record: A version of this preprint was published on January 11th, 2021. See the published version at https://doi.org/10.1186/s40623-020-01349-1.

Title: Locating hydrothermal fluid injection of the 2018 phreatic eruption at Kusatsu-Shirane volcano with volcanic tremor amplitude

Author #1: Taishi Yamada, Sakurajima Volcano Research Center, Disaster Prevention Research Institute, Kyoto University, 1722-19 Sakurajima-Yokoyama, Kagoshima 891-1419, Japan, yamada.taishi.8m@kyoto-u.ac.jp

Author #2: Aika, K. Kurokawa, National Research Institute for Earth Science and Disaster Resilience, Tennodai 3-1, Tsukuba, Ibaraki 305-0006, Japan

Author #3: Akihiko Terada, Volcanic Fluid Research Center, School of Science, Tokyo Institute of Technology, 2-12-1 Ookayama, Meguro, Tokyo 152-8551, Japan

Author #4: Wataru Kanda, Volcanic Fluid Research Center, School of Science, Tokyo Institute of Technology, 2-12-1 Ookayama, Meguro, Tokyo 152-8551, Japan

Author #5: Hideki Ueda, National Research Institute for Earth Science and Disaster Resilience, Tennodai 3-1, Tsukuba, Ibaraki 305-0006, Japan

Author #6: Hiroshi Aoyama, Institute of Seismology and Volcanology, Faculty of Science, Hokkaido University, N10W8, Kita-ku, Sapporo, Hokkaido 060-0810, Japan

Author #7: Takahiro Ohkura, Aso Volcanological Laboratory, Kyoto University, 3028 Sakanashi, Ichinomiya-machi, Aso, Kumamoto 869-2611, Japan

Author #8: Yasuo Ogawa, Volcanic Fluid Research Center, School of Science, Tokyo Institute of Technology, 2-12-1 Ookayama, Meguro, Tokyo 152-8551, Japan

Author #9: Toshikazu Tanada, National Research Institute for Earth Science and Disaster Resilience, Tennodai 3-1, Tsukuba, Ibaraki 305-0006, Japan

Correspondence: Taishi Yamada (yamada.taishi.8m@kyoto-u.ac.jp)

*Table 1 is placed at the end of this file.

Abstract

Kusatsu-Shirane volcano has been a particular study field for hydrothermal system and phreatic eruptions with plenty of thermal springs, fumaroles, and a crater lake of Yugama. On 23 January 2018, a phreatic eruption occurred at the Motoshirane cone of Kusatsu-Shirane, where no considerable volcanic activity had been reported in observational and historical records. To understand the eruption process of such a unique event, we examined observed seismic, tilt, and infrasound records. The onset of surface activity accompanied by infrasound signal was preceded by volcanic tremor and inflation of the volcano for 2 minutes. Tremor signals with a frequency of 5–20 Hz remarkably coincide with the rapid inflation. We apply an amplitude source location method to seismic signals in the 5–20 Hz band to estimate tremor source locations. Our analysis locates tremor sources at 1 km north of Motoshirane and at a depth of 0.5–1 km from the surface. Inferred source locations correspond a conductive layer of impermeable cap-rock estimated by magnetotelluric investigations, and an upper portion of the seismogenic region, suggesting hydrothermal activity hosted beneath the cap-rock. Examined seismic signals in the 5–20 Hz band are typically excited by

volcano-tectonic events with faulting mechanism. Based on the above characteristics and background, we interpret that excitation of examined volcanic tremor reflects small shear fractures induced by sudden hydrothermal fluid injection to the cap-rock layer. The horizontal distance of 1 km between inferred tremor sources and Motoshirane implies lateral migration of the hydrothermal fluid, although we have not obtained direct evidence. Kusatsu-Shirane has a series of unrest at the Yugama lake since 2014. However, inferred tremor source locations do not overwrap active seismicity beneath Yugama. Therefore, our result suggests that the 2018 eruption was triggered by hydrothermal fluid injection through an independent pathway that has driven unrest activities at Yugama.

Keywords

Kusatsu-Shirane, Phreatic eruptions, Volcanic tremor, Hydrothermal system

Main Text

Introduction

Kusatsu-Shirane volcano consists of three pyroclastic cones (Shirane, Ainomine, and Motoshirane), central Japan (Fig. 1). A distinguishing characteristic of Kusatsu-Shirane is a well-developed hydrothermal system beneath the volcano, evidenced by a significant amount of thermal springs, fumaroles, and a crater lake (Yugama) at the summit of the Shirane cone. Therefore, it has been a particular study field of volcano hydrothermal system and phreatic eruptions (e.g., Ossaka et al., 1980; Ohba et al., 1994; Terada and Hashimoto, 2017; Terada 2018). On 23 January 2018, a phreatic eruption occurred at Kusatsu-Shirane, and several small craters with diameters of 15–20 m have been formed at the summit area of the Motoshirane cone (Earthquake Research Institute, 2018). A unique point of the 2018 eruption is that the event occurred at Motoshirane because all documented (after 1882) phreatic eruptions and recent unrest events in the period of 1989–1991 and 2014 have occurred at the Shirane cone (Terada, 2018). No considerable precursory changes related to Motoshirane had been reported before the event. As well as the 2018 Kusatsu-Shirane eruption, phreatic eruptions are not always accompanied by clear precursors (Barberi et al., 1992). Assessing the potential of upcoming phreatic eruptions is an important

challenge for volcano research and monitoring. Hence, case studies for each event are still significant to improve our understanding of the phreatic eruption mechanism (e.g., Mannen et al., 2018; Ueda et al., 2018; Stix and de Moor, 2018; Battaglia et al., 2019).

Phreatic eruptions may be regarded as relatively small events from a view of the total ejected material amount (VEI: Volcano Explosive Index, Newhall and Self, 1992), with the VEI of 0–2 (e.g., Brown and Lawless, 2001; Mayer et al., 2015; Maeno et al., 2016; Geshi and Itoh, 2018; Mannen et al., 2018, The Joint Research Team for ash fall in Kusatsu-Shirane 2018 eruption, 2018). However, phreatic eruptions and related unrest activities often excite seismic signals and transient ground deformation with considerable amplitudes (e.g., Aoyama and Oshima, 2008; Maeda et al., 2015; Aoyama and Oshima, 2015). Previous studies have demonstrated that seismic analysis is vital for understanding the phreatic eruption mechanism and related hydrothermal activities with locations, force system, and its temporal changes of seismic wave sources (e.g., Jolly et al., 2010; Kato et al., 2015; Maeda et al., 2015; Yukutake et al., 2017; Jolly et al., 2018). Amplitude Source Location (ASL) method has been applied at a lot of volcanoes to constrain the source location of volcanic tremor (e.g., Yamasato,

1997; Battaglia and Aki, 2003, Kumagai et al., 2010; Kurokawa et al., 2016; Ichihara and Matsumoto, 2017; Ichimura et al., 2018; Walsh et al., 2019). Since no investigation has been reported at Motoshirane in terms of geophysical ground observations, our primal objective is to locate where the hydrothermal fluid that drove the 2018 phreatic eruption came from. We apply the ASL technique to seismic records accompanying the 2018 eruption to estimate source locations of volcanic tremor. The relation between our result and the hydrothermal system structures of Kusatsu-Shirane are discussed to obtain an illustration of the source process of the 2018 eruption.

Observation networks

Kusatsu-Shirane Volcano Observatory (KSVO), Volcano Fluid Research Center, Tokyo Institute of Technology, has operated the seismic observation network at Kusatsu-Shirane since 1990 (Mori et al., 2006). The seismic network of KSVO focuses on the Shirane cone where has the most active seismicity in Kusatsu-Shirane (Fig. 1c). We adopt seismic data recorded at KSE, KSS, KSW, KSYG, and JIE, and infrasound data at KSRH. National Research Institute for Earth Science and Disaster Resilience (NIED) also

has the multiparametric observation network (V-net) at Kusatsu-Shirane since 2014 (Tanada et al., 2017). Seismic and tilt data obtained by borehole instruments at KSHV, KSYV, and KSNV (Fig. 1b) are adopted in this paper. We also analyze ground velocity and infrasound data recorded at KSAO, KSHA, and KSAO (Fig. 1c), operated by Japan Meteorological Agency (JMA). All analyzed seismic data were recorded by seismometers with a natural frequency of 1 Hz. Details of our dataset are summarized in Table 1.

Seismicity and hydrothermal system structures at Kusatsu-Shirane

Hypocenter distributions of volcanic earthquakes at Kusatsu-Shirane routinely determined by KSVO are shown in Fig. 2a. Two earthquake clusters characterize the seismicity at Kusatsu-Shirane: the major one is beneath the Yugama lake (Yugama cluster) extending in the elevation range of 500–1700 m. Most events in Fig. 2 are Volcanic Tectonic (VT) type, although some events in the Yugama cluster are recognized as Long-Period (LP) events which having a fluid-driven mechanism (Nakano et al., 1998; Kumagai et al., 2002; Fujita and Ida, 2003; Nakano et al., 2003). Another

cluster can be found beneath the Ainomine cone (Ainomine cluster). Since no seismic station covers the south of Ainomine in a close range (Fig. 1 and 2) up to the 2018 eruption (Yamamoto et al., 2018), the precision of hypocenter determination for the Ainomine cluster may be less than that of the Yugama cluster. The number of volcanic earthquakes significantly decreases below sea level. Audio-magnetotelluric (AMT) (Nurhasan et al. 2006) and magnetotelluric (MT) surveys (Matsunaga et al., 2020; Tseng et al., under review) detect a conductive region at a depth of 1–3.5 km from the surface, which almost corresponds low seismicity region in Fig. 2a. The conductor is interpreted as a hydrothermal fluid reservoir that is the origin of thermal springs, fumaroles, and lake waters at Kusatsu-Shirane inferred by geochemical studies (Hirabayashi, 1999; Ohba et al., 2000; Ohwada et al., 2003). Therefore, a plausible interpretation for seismicity above the fluid reservoir is that ascending hydrothermal fluid induces small earthquakes (Nurhasan et al., 2006; Tseng et al., under review). The Motoshirane cone had the latest lava effusion at the Kusatsu-Shirane 1500 years ago (Nigorigawa et al., 2016). Besides, some small craters at the summit area of Motoshirane may suggest the possibility of unconfirmed phreatic eruptions after the

last lava effusion (Fig. 1c, Geospatial Information Authority of Japan, 2018). The flank of the Motoshirane produces thermal springs with the total discharge energy of 110 MW (Ueki and Terada, 2012). Although this value is considerably large for non-eruptive volcanism (Kagiyama, 1981), no remarkable seismic activities are found in Fig. 2a.

Focusing on volcanic activity of Kusatsu-Shirane in the last decades, the first unique event after the 1989–1991 unrest (Takahashi and Fujiwara, 2014; Terada 2018) is a transient ground inflation-deflation event accompanying volcanic tremor on January 2011 (the 2011 unrest) beneath the Ainomine peak (Terada et al., 2011; Fujiwara et al., 2011). From March 2014, major seismic swarms started around Yugama (Kuwahara et al., 2016), along with ground inflation, changes in the total magnetic field, temperature, and geochemical components in lake water of Yugama (Terada et al., 2016; Ohba et al., 2016). Figure 2b shows the time history of seismicity at Kusatsu-Shirane from June 2016 to December 2018. The beginning of the time window in Fig. 2b corresponds that a series of unrest from 2014 had been gradually diminishing. Apart from the phreatic eruption on 23 January 2018, a new series of the

seismic swarm has begun at Yugama from April 2018. No eruption related to this unrest occurred up to May 2020 (JMA, 2020).

The 2018 phreatic eruption

We plot seismic, tilt, and infrasound records from 09:58 to 10:05 on 23 January 2018 (JST) including signals accompanying the 2018 eruption in Fig. 3. Volcanic tremor appears on a raw ground velocity record at KSW from 9:59:35 (Fig. 3a). Tremor amplitude once decreases from 10:01:30, and another wave group follows with a larger amplitude (10:02:10). Fourier spectra of seismic signals in Fig. 3a (from 09:58:20) and background signals before the onset of tremor (from 09:50:00) are denoted in Fig. 4a. The frequency content of seismic signals associated with the 2018 eruption has broad peak ranges from 0.5 Hz to 30 Hz. A better view for understanding the frequency content is obtained from amplitude ratios to background time window in Fig. 4b. We see that there are two major signal peaks in frequency bands of 1–2 Hz and 4–30 Hz. To examine temporal intensity changes of each peak band, causal band-pass filters with two corresponding cut-off frequency bands (0.5–5 Hz, and 5–20 Hz)

are applied on raw vertical ground velocity in Fig 3b. A filtered waveform in the 0.5–5 Hz band has an almost identical time history with a raw waveform. On the other hand, another filtered (5–20 Hz) waveform shows a different time series of amplitude; It has signals with a considerable amplitude on 09:59–10:01 as well as raw and the 0.5–5 Hz filtered waveforms but has fewer signals on the second impulsive wave group from 10:02:10.

Tilt records at KSHV are shown in Fig. 3c. To emphasize dynamic ground deformation, an acausal low-pass filter with a cut-off frequency of 0.05 Hz is applied on tilt records in Fig. 3c. We see that an east-northward uplift begins almost simultaneous with volcanic tremor. Since the station KSHV is located on the west-southwest side flak of Motoshirane, the tilt change from 10:00 can be interpreted as inflation of the Motoshirane cone, as well as other tilt records accompanying the 2018 eruption (Terada et al., 2018). The polarity of tilt change turns to the opposite at 10:01:50. This timing corresponds that the amplitude of the first tremor from 09:59 decreases. We also plot the cumulative squared amplitude of filtered (5–20 Hz) vertical ground velocity at KSW in Fig. 3c. Both volcanic tremor in the 5–20 Hz band and the

inflation occur in an almost identical time window.

Figure 3d shows the raw infrasound waveform at KSRH. Although the waveform contains noise signals probably derived from wind, there is a characteristic wave group from 10:02:13 with a greater amplitude than the background level. To examine the origin time of this infrasound, we plot raw infrasound records at KSRH and KSAO from 10:02:00 in Fig. 5. Although signal-to-noise ratio (SNR) of infrasound record at KSAO is relatively low, we find coherent signals on both infrasound waveforms from 12 s in Fig. 5. Arrival times of signals in both waveforms can be explained assuming that the signals propagate from the center of main vents of the 2018 eruption (Fig. 2a) with an apparent velocity of 340 m/s, which is consistent with the sound velocity near the ground. Hence, we consider the origin time of infrasound is 10:02:09. This is consistent with a report by ERI (2018), who examined the coherence of seismic and infrasound signals (Ichihara et al., 2012). The infrasound origin time also implies that the excitation of the second wave group on seismic record (Fig. 3a) is associated with surface activity with ash and gas emissions.

The 2018 eruption affected the local electricity supply network with ashfall,

and it caused data loss at KSE, JIE, KSYG, and KSHA after 10:02:40. Therefore, we focus on the time window for 210 s from 09:50:10 in the following sections.

ASL method for the 2018 eruption

Our inspection of observed data associated with the 2018 eruption shows that volcanic tremor precedes the onset of eruption for 2 minutes. Now we apply the ASL technique to seismic record to estimate volcanic tremor source locations. Here, analyzed seismic signals are assumed as body waves from a point source, and having an isotropic radiation pattern with wave scattering in the medium.

Based on the assumption, ground velocity amplitude at r_i km away from the seismic source, $A(r_i)$, can be expressed as

$$A(r_i) = \frac{A_0 S_i}{r_i} exp(-Br_i), \qquad B = \frac{\pi f}{\beta Q}, \tag{1}$$

where A_0 is source amplitude, S_i is site amplification factor, f is the center frequency of analyzed signals, β is the *S*-wave velocity in the medium, and Q is the

quality factor for medium attenuation (Aki and Richards, 2002). The subscript *i* corresponds at the *i*–th station in the network. The assumption for isotropic *S*-wave radiation is effective for signals with frequencies higher than 5 Hz (Takemura et al., 2009; Kumagai et al., 2011). Hence, we focus on ground velocity in the band of 5–20 Hz, which is almost identical to one of the dominant frequency ranges in observed seismic records. A homogeneous *S*-wave velocity of $\beta = 2.42$ km/s is referred from Kuwahara et al. (2016), who examined seismic velocity structures at Kusatsu-Shirane with travel times of volcanic earthquakes. The quality factor Q is set 50 as a representative value at active volcanoes (e.g., Koyanagi et al., 1995; Battaglia and Aki, 2003; Morioka et al., 2017). We adopt seismic records at KSE, KSS KSW, KASO, and KSHA in the ASL based on considering the SNR, distances from the Motoshirane cone, and operational history including the 2011 unrest. The ASL determines the source location by minimizing residuals between observed and modeled amplitudes by Equation 1. However, since no seismic station covers the south of Motoshirane, grid-search for the minimum residual needs to be modified to suit our network configuration. Hence, we follow an improved version of the ASL proposed by Ichihara

and Matsumoto (2017) for searching the minimum residual and S_i determination. Their method evaluates residuals with amplitude ratios of each station pairs. Ratios of observed (R_{ij}^{obs}) and modeled (R_{ij}^{model}) amplitudes from Equation 1 of each station pair are defined as

$$R_{ij}^{\mathrm{obs}} = \frac{A_i^{\mathrm{obs}}}{A_j^{\mathrm{obs}}}, \qquad R_{ij}^{\mathrm{model}} = \frac{S_i r_i^{-1} \exp\left(-B r_i\right)}{S_j r_j^{-1} \exp\left(-B r_j\right)}, \tag{2}$$

where A_i^{obs} is a band-passed Root-Mean-Squared (RMS) amplitude in each time window for 10 s. By adopting Equation 2 for grid-search, observed seismic traces at relatively distant stations with smaller amplitudes can contribute to minimizing residuals equally as well as traces with larger amplitudes. Diminishing a parameter of A_0 in Equation 2 improves the robustness of the analysis. Therefore, we consider the error evaluation with amplitude ratio is better than that with amplitude only (Battaglia and Aki, 2003). The residual between observed and modeled amplitude ratios is defined as

$$RES = \sqrt{\frac{2}{N(N-1)} \sum_{i=1}^{N-1} \sum_{j=i+1}^{N} \left(\frac{R_{ij}^{\mathrm{obs}} - R_{ij}^{\mathrm{model}}}{R_{ij}^{\mathrm{obs}}} \right)^2}. \quad (3)$$

Each time window is shifted for 10 s without overwrapping each other.

Equation 1 shows that S_i at each station is critical for source location determination with the ASL. Values of S_i are usually determined with a coda-normalization method using far-field earthquakes (Phillips and Aki, 1986; Mayeda et al., 1991). However, amplitude variations of observed coda-wave affect the estimation of S_i, and it causes potential errors for source location estimates (Ogiso et al., 2016; Walsh et al., 2017). Following Ichihara and Matsumoto (2017), the present study determines S_i setting a reference time window that the source location is fixed at a certain point. In our case, a reference window is set from 10:02:10 with source location at the surface of the center of main vents (Fig. 2a), because this time window includes the origin time of dominant infrasound signals. Figure 6a shows RES values for the reference time window with different reference source elevations beneath the vent without considering S_i (setting S_i as 1). Since the minimum value of RES is obtained at the ground surface (an elevation of 2050 m) in Fig. 6, we consider the

assumption of fixed source location in the reference time window is acceptable. Corresponding modeled amplitudes by Equation 1 are denoted in Fig. 6b with observed filtered RMS amplitudes of the reference time window at each station. The source amplitude of A_0 is calculated to explain observed RMS amplitude at KSW for each grid node and time window. This choice of KSW for A_0 determination is based on that the borehole instrument at KSW is set in the host rock (Uto et al., 2004), and that vertical seismic records at KSW show the lowest amplification in the network with the coda-normalization method (Table S2). Hence, S_i at other stations is determined to satisfy the modeled amplitudes in the reference time window in Fig. 6b.

Searching for the minimum RES is conducted with a grid size of 10 m. We set a search range from elevations of −1500 m to the surface, latitudes of 36.618–36.651, and longitudes of 138.524–138.558, which covers almost whole Motoshirane and Shirane cones.

Result

Figure 7a represents horizontal tremor locations obtained by our ASL analysis. The

color of each plot indicates the time as shown in a color palette of Fig. 7b. Filtered (5–20 Hz) vertical ground velocity at KSW, estimated source elevation, and the minimum RES value of each time window are denoted in Fig. 7b. A source location plot surrounded by a green square (190 s) is the reference window that the source is fixed at the surface of the vent. Inferred tremor locations up to 170 s are ranging about 500 m east of the Ainomine peak. Corresponding elevations are in the range of 1.0–1.5 km, which is equivalent to a depth of 0.5–1 km from the ground surface. Inferred source locations suddenly move to the south in 180 s. After the reference window in 190 s, source locations are estimated at near the ground surface around Motoshirane. For evaluating the reliability of source location estimates, Fig. 8 shows an example of the distribution of RES in horizontal and vertical cross-sections of a time window of 120 s as a representative in Fig. 7. If we set an error range of 0.1 > RES, the range corresponds −110–130 m in the NS direction, and −50–60 m in the EW direction in horizontal cross-section. On the other hand, the error range in vertical cross-sections becomes −200–300 m. One possible explanation of relatively poor constraint on source elevation may be derived from the station configuration regardless of our

improvement of the ASL method. Therefore, inferred tremor source elevations may include potential errors with several hundred meters.

We also conduct the ASL analysis with different *S*-wave velocity and Q values to assess how our ASL depends on those elastic media parameters. If we adopt β as 1.43 km/s from Ida et al., (1989), the ASL yields source location at an elevation of 40 m higher, and 70 m south away from the result in the window of 120 s in Fig. 8. Adopting different Q values (40 and 60) changes inferred source locations for $\pm$30 m. Therefore, we consider the dependence on the elastic media parameters is limited.

To validate our determination of S_i at each station, we also conduct the ASL with S_i obtained with the coda-normalization method with different station configuration (Fig. S2). Although estimated tremor elevations are unstable in time, the horizontal tremor locations are identical to those of the main result in Fig. 7. Therefore, we convince that our ASL method yields reasonable results.

Discussion

Interpretation for examined volcanic tremor and eruption process

Seismic signals in the 5–20 Hz band that adopted in our ASL are usually excited by VT events with faulting mechanisms at active volcanoes (Nishimura and Iguchi, 2011). Figure 4b shows a considerable agreement of frequency content between examined volcanic tremor and a VT event after the eruption (10:14). Considering this correspondence of frequency content, we assume that the 5–20 Hz band seismic signals of volcanic tremor are a superposition of signals excited by small shear fractures. Based on this hypothesis, the corner frequency, f_c, of each fracture may be estimated as 10–20 Hz from Fig. 4. This f_c range is equivalent to seismic moment (M_0) of 10^{11}–10^{13} Nm following a scaling of $M_0 \propto f_c^{-3}$ (Hiramatsu et al., 2002). A compilation by Abercrombie (1995) demonstrates that fault slips with M_0 of 10^{11}–10^{13} Nm are expected to have fault radii of < 100 m, which is comparable to variations of the inferred source locations by our ASL beneath Ainomine. Therefore, small shear fractures can be a plausible source mechanism of examined signals in the ASL. On the other hand, the behavior of hydrothermal fluid itself can excite ground velocity. Since geysers and fumaroles can excite seismic signals with frequencies higher than 10 Hz (Motoya and Nogoshi, 1962; Kedar et al., 1996), a superposition of fault slips may not

be a unique mechanism for hydrothermal related seismic signals. However, ideas of seismic wave excitation related to hydrothermal fluid behavior are often applied to signals with lower frequency ranges of < 0.5 Hz (e.g., Fujita and Ida, 2003; Ohminato, 2006; Maeda et al., 2013). This signal range also corresponds to another frequency peak of observed ground velocity associated with the 2018 eruption (Fig. 4), although we do not focus on this paper. Hence, we prefer small shear fractures as a mechanism of examined tremor signals.

Our ASL method estimates volcanic tremor source locations at about 500 m east and the depth of 0.5–1 km beneath the Ainomine cone. This region corresponds slightly east, and an upper portion of the Ainomine cluster (Fig. 2). Hypocenters of volcanic earthquakes with different station configuration and seismic velocity model from the present routine of KSVO is reported by Mori et al. (2006). Their result has almost the same epicenter distributions with tremor locations by our ASL. Note that inferred tremor locations are relative to the reference point that is fixed at the surface of the vent. However, the comparison between our result and hypocenter distributions significantly suggests that excitations of examined volcanic tremor relate

to the seismogenic zone beneath Ainomine. According to AMT and MT soundings, the eastern flank of Kusatsu-Shirane is covered by a conductive layer with a thickness of 0.3–1 km (Nurhasan et al. 2006; Matsunaga et al., 2020; Tseng et al., under review). Drillings reveal that the conductive layer consists of smectite with an impermeable characteristic (Kurasawa, 1993). A low permeable structure, often known as cap-rock, is essential to seal vertical fluid flow for hosting a hydrothermal system. The sealing structure by the cap-rock beneath Ainomine can be supported by the focal depth of volcanic earthquakes. Most earthquakes in the Ainomine cluster occur below an elevation of 1 km (Fig. 2). This can be interpreted that low seismicity reflects less hydrothermal fluid ascends in the cap-rock layer, and hosted hydrothermal fluid beneath the cap-rock induces the seismicity beneath the Ainomine. Based on the above signal characteristics and background, it is plausible to assume that sudden and unusual hydrothermal fluid injection for the cap-rock layer beneath Ainomine occurred, and that induced the small shear fractures in the cap-rock observed as volcanic tremor (Fig. 9).

One of the important features of analyzed seismic signals in the 5–20 Hz

band is that it is accompanied by the rapid inflation. Volcanic tremor accompanying ground deformation is widely reported associated with phreatic eruptions and unrests at other volcanoes, such as Kuchinoerabujima (Tameguri et al., 2016; Nakamichi et al., 2016), Ontake (Kato et al., 2015), Hakone (Honda et al., 2018; Yukutake et al., 2018), Meakan-dake (Aoyama and Oshima, 2008; Aoyama and Oshima, 2015), and Hokkaido-Komagatake (Usu Volcano Observatory, 1997). Such sudden ground inflation is often inferred as an expansion of super-heated underground water, which can be a possible trigger of phreatic eruptions (Maeda et al., 2017; Stix and de Moor, 2018). Himematsu et al., (2020) detected syn-eruptive and post-eruptive subsidence of Motoshirane with Synthetic Aperture Radar (SAR) data. Although we do not estimate deformation source location with tilt records in this paper, ground deformation obtained with the spaceborne observation by Himematsu et al. (2020) suggests that the deformation source beneath the Motoshirane induced the tilt change. Therefore, a possible scenario to explain observed volcanic tremor and ground inflation is that injected hydrothermal fluid beneath Ainomine migrated laterally at a certain depth, and induced the deformation beneath Motoshirane (Fig. 9).

Implications for the hydrothermal system structure of Kusatsu-Shirane volcano

The Yugama and Ainomine clusters of volcanic earthquakes have been recognized from seismic observation in the 1980s (Ida et al., 1989). Ida et al. (1989) interpreted that the Ainomine cluster can be a part of the fluid pathway from source to beneath Yugama, considering the difference in the focal depth of both clusters. Along with seismic records of the 2018 eruption, we also apply the same ASL analysis to seismic records of the 2011 unrest (Fig. S3). Inferred tremor locations are almost identical to that of the 2018 eruption, which does not overwrap the Yugama cluster. This can be interpreted that the 2011 unrest share the same triggering with the 2018 eruption. The relation between both seismic clusters can be discussed from the time series of seismicity. Figure 2 shows no clear changes in the Yugama cluster related to the 2018 eruption at Motoshirane. Similarly, the Ainomine cluster has no response to a series of unrest at the Yugama since April 2018. Therefore, it is reasonable to consider that both seismic clusters reflect the existence of independent hydrothermal fluid pathways from the fluid reservoir (Fig. 9). Such a perspective can contribute evaluation of

volcanic activity at Kusatsu-Shirane.

Our result reveals a major triggering system of the 2018 eruption is located not beneath Motoshirane, but Ainomine. This may be consistent with low seismicity beneath Motoshirane in the time window in Fig. 2b. However, the present study does not show the nature of the horizontal distance between the vent (Motoshirane) and triggering hydrothermal fluid injection (beneath Ainomine). We also blind about the condition beneath the Motoshirane before the eruption, because few ground observations had focused on the Motoshirane cone. Previous studies at Kusatsu-Shirane have revealed some fundamental aspects of the hydrothermal system focusing on the Shirane cone. Further investigations and continuous observation targeting Motoshirane, as well as Shirane, will benefit to obtain better understandings of the hydrothermal system beneath Kusatsu-Shirane volcano.

Conclusion

We have examined seismic, tilt, and infrasound records accompanying the 2018 phreatic eruption at Kusatsu-Shirane volcano to understand the source process of a

unique eruption after a long dormancy of the Motoshirane cone. Our dataset shows the onset of eruption characterized by infrasound signal is preceded by volcanic tremor and tilt change for 2 minutes. One of the important characteristics of the volcanic tremor is that signals in the 5–20 Hz band are accompanied by rapid inflation. We applied the ASL method for the 5-20 Hz band signals to determine tremor source locations. Our analysis estimates the tremor sources at 1 km north from Motoshirane and at a depth of 0.5–1 km. Inferred source locations correspond to an impermeable cap-rock layer and an upper portion of the seismogenic region beneath the Ainomine cone. Seismic signals in the 5-20 Hz band correspond dominant signals accompanying VT events with faulting mechanism. Therefore, we interpret that examined volcanic tremor reflects small shear fractures induced by sudden hydrothermal fluid injection for the cap-rock layer, and that triggered the 2018 eruption. Our investigation also suggests that the hydrothermal fluid injection occurred at an independent pathway from that beneath the Shirane cone, which has driven a series of unrest since 2014 at Yugama.

Declarations

Ethics approval and consent to participate

Not applicable.

Consent for publication

Not applicable.

List of abbreviations

ASL: Amplitude Source Location; KSVO: Kusatsu-Shirane Volcano Observatory; NIED: National Research Institute for Earth Science and Disaster Resilience; JMA: Japan Meteorological Agency; VT: Volcano Tectonic; LP: Long Period; JST: Japan Standard Time; RMS: Root-Mean-Squared; GSI: The Geospatial Information Authority of Japan; AMT: Audio-magnetotelluric; MT: Magnetotelluric; SNR: signal-to-noise ratio

Availability of data and materials

Seismic and tilt data from NIED and JMA can be downloaded from https://www.vnet.bosai.go.jp.

Competing interests

All authors have no competing interests.

Funding

The present study was partly supported by the Ministry of Education, Culture, Sports, Science, and Technology (MEXT) of Japan, under its Earthquake and Volcano Hazards Observation and Research Program, Integrated Program for Next Generation Volcano Research and Human Resource Development.

Authors' contributions

TY and AK conducted the ASL analysis for seismic data. AT, WK, and YO are in charge of continuous observation of KSVO. HA and TO have been assisted for observation and data processing of KSVO. HU, TT, and TY are involved in operating of V-net at Kusatsu-Shirane. The initial outlines of this study have been discussed by TY, AT, and HA. All authors read and approved the manuscript.

Acknowledgments

Staffs of KSVO are grateful for their contribution to the continuous operation of the observation network. Discussions with Profs. Junichi Hirabayashi and Masato Iguchi were valuable for giving interpretation for our result. JMA and GSI are acknowledged for providing observation data and digital elevation map at Kusatsu-Shirane volcano. Details of instruments information of JMA was provided by Dr. Ryohei Kawaguchi in Meteorological Research Institute, JMA.

References

Abercrombie RE (1995) Earthquake source scaling relationships from -1 to 5 ML using seismograms recorded at 2.5-km depth. J Geophys Res Solid Earth 100:24,015–24,0365. https://doi.org/10.1029/95jb02397.

Aki K, Richards PG (2002) Quantitative Seismology. 2nd edn. University Science Books, Sausalito, USA

Aoyama H, Oshima H (2008) Tilt change recorded by broadband seismometer prior to small phreatic explosion of Meakan-dake volcano, Hokkaido, Japan. Geophys Res Lett 35:L06307. https://doi.org/10.1029/2007GL032988.

Aoyama H, Oshima H (2015) Precursory tilt changes of small phreatic eruptions of Meakan-dake volcano, Hokkaido, Japan, in November 2008. Earth Planets Space 67:119. https://doi.org/10.1186/s40623-015-0289-9.

Barberi F, Bertagnini A, Landi P, Principe C (1992) A review on phreatic eruptions and their precursors. J Volcanol Geotherm Res 52:231–246. https://doi.org/10.1016/0377-0273(92)90046-G.

Battaglia J, Aki K. Location of seismic events and eruptive fissures on the Piton de la Fournaise Volcano using seismic amplitudes. J Geophys Res 2003;108:2364. doi:10.1029/2002JB002193.

Battaglia A, de Moor JM, Aiuppa A, et al (2019) Insights into the mechanisms of phreatic eruptions from continuous high frequency volcanic gas monitoring: Rincón de la Vieja Volcano, Costa Rica. Front Earth Sci 6:1–20. https://doi.org/10.3389/feart.2018.00247.

Browne PRL, Lawless J V. (2001) Characteristics of hydrothermal eruptions, with examples from New Zealand and elsewhere. Earth Sci Rev 52:299–331. https://doi.org/10.1016/S0012-8252(00)00030-1

Earthquake Research Institute (2018) Kusatsu-shirane, Report of Coordinating Committee for Prediction of Volcanic Eruption No.140. Jpn Meteorol Agency, Tokyo. https://www.data.jma.go.jp/svd/vois/data/tokyo/STOCK/kaisetsu/CCPVE/shiryo/140/140_01-1-2.pdf. Accessed 15 July 2020 (in Japanese).

Fujita E, Ida Y, Oikawa J (1995) Eigen oscillation of a fluid sphere and source

mechanism of harmonic volcanic tremor. J Volcanol Geotherm Res 69:365–378. https://doi.org/10.1016/0377-0273(95)00027-5.

Fujita E, Ida Y (2003) Geometrical effects and low-attenuation resonance of volcanic fluid inclusions for the source mechanism of long-period earthquakes. J Geophys Res Solid Earth 108:1–17. https://doi.org/10.1029/2002jb001806.

Fujiwara Y, Yamasato H, Ogiso M (2011) Sources of the volcanic tremor with tilt changes on 27 May 2011 at Kusatsu-Shiranesan estimated using seismic amplitudes. Abstracts of the Volcanological Society of Japan 2015 Fall Meeting: P24 (in Japanese).

Geospatial Authority of Japan (2018) Information of volcanic activity at Kusatsu-Shirane volcano. https://www.gsi.go.jp/BOUSAI/kusatsushirane-index.html. Accessed 19 July 2020 (in Japanese).

Geshi N, Itoh J (2018) Pyroclastic density currents associated with the 2015

phreatomagmatic eruption of the Kuchinoerabujima volcano. Earth Planets Sp 70:119. https://doi.org/10.1186/s40623-018-0881-x.

Himematsu Y, Ozawa T, Aoki Y (2020) Coeruptive crustal deformation associated with the 2018 Kusatsu-Shirane phreatic eruption based on PALSAR-2 time-series analysis. Earth Planets Sp 72:116. https://doi.org/10.1186/s40623-020-01247-6.

Hirabayashi J (1999) Formation of volcanic fluid reservoir and volcanic activity. J Hot Spring Sci 49:99–105 (in Japanese).

Hiramatsu Y, Yamanaka H, Tadokoro K, et al (2002) Scaling law between corner frequency and seismic moment of microearthquakes: Is the breakdown of the cube law a nature of earthquakes. Geophys Res Lett 29:8–11. https://doi.org/10.1029/2001GL013894.

Honda R, Yukutake Y, Morita Y, et al (2018) Precursory tilt changes associated with a

phreatic eruption of the Hakone volcano and the corresponding source model. Earth Planets Sp 70:117. https://doi.org/10.1186/s40623-018-0887-4.

Ichihara M, Matsumoto S (2017) Relative Source Locations of Continuous Tremor Before and After the Subplinian Events at Shinmoe-dake, in 2011. Geophys Res Lett 44:10,871–10,877. https://doi.org/10.1002/2017GL075293.

Ichimura M, Yokoo A, Kagiyama T, et al (2018) Temporal variation in source location of continuous tremors before ash–gas emissions in January 2014 at Aso volcano, Japan. Earth Planets Sp 70:125. https://doi.org/10.1186/s40623-018-0895-4.

Ida Y, Osada N, Sawada M, Koyama E, Kagiyama T (1989) Seismological study based on recently installed permanent stations and a small eruptive event on January 6, 1989 at Kusatsu-Shirane volcano. Bull Earth Res Inst 64:325–345 (in Japanese with English abstract).

Iguchi M, Nishimura T (2011) Volcanic Earthquakes and Tremor in Japan. Kyoto Univ Press, Kyoto, Japan.

Japan Meteorological Agency (2020) Kusatsu-shirane. Paper presented at 146th Meeting of Coordinating Committee for Prediction of Volcanic Eruptions. Jpn Meteorol Agency, Tokyo. https://www.data.jma.go.jp/svd/vois/data/tokyo/STOCK/kaisetsu/CCPVE/shiryo/146/146_1-1.pdf. Accessed 15 July 2020 (in Japanese).

Jolly AD, Sherburn S, Jousset P, Kilgour G (2010) Eruption source processes derived from seismic and acoustic observations of the 25 September 2007 Ruapehu eruption-North Island, New Zealand. J Volcanol Geotherm Res 191:33–45. https://doi.org/10.1016/j.jvolgeores.2010.01.009.

Jolly A, Lokmer I, Christenson B, Thun J (2018) Relating gas ascent to eruption triggering for the April 27, 2016, White Island (Whakaari), New Zealand eruption

sequence. Earth Planets Sp 70:1–15. https://doi.org/10.1186/s40623-018-0948-8.

Kagiyama T (1981) Evaluation methods of heat discharge and their applications to the major active volcanoes in Japan. J Volcanol Geotherm Res. 9:87–97. https://doi.org/10.1016/0377-0273(81)90016-0.

Kato A, Terakawa T, Yamanaka Y, et al (2015) Preparatory and precursory processes leading up to the 2014 phreatic eruption of Mount Ontake, Japan. Earth Planets Sp 67:111. https://doi.org/10.1186/s40623-015-0288-x.

Kedar S, Sturtevant B, Kanamori H (1996) The origin of harmonic tremor at Old Faithful geyser. Nature 379:708–711. https://doi.org/10.1038/379708a0.

Koyanagi S, Aki K, Biswas N, Mayeda K (1995) Inferred attenuation from site effect-corrected T phases recorded on the island of Hawaii. Pure Appl Geophys 144:1–17. https://doi.org/10.1007/BF00876471.

Kuwahara T, Terada A, Yukutake Y, Kanda W, Ogawa Y (2016) Upward fluid migration accompanying earthquake swarms at Kusatsu-Shirane volcano in 2014. Abstracts of the Volcanological Society of Japan 2016 Fall Meeting: B3-23 (in Japanese).

Kumagai H, Chouet BA, Nakano M (2002) Waveform inversion of oscillatory signatures in long-period events beneath volcanoes. J Geophys Res Solid Earth 107(B11):2301. https://doi.org/10.1029/2001jb001704.

Kumagai H, Saito T, O'Brien G, Yamashina T (2011) Characterization of scattered seismic wavefields simulated in heterogeneous media with topography. J Geophys Res Solid Earth 116:1–13. https://doi.org/10.1029/2010JB007718.

Kurasawa T (1993) Problem with the Drilling of Geothermal Well in the South of Mt. Kusatsu-Shirane, Gunma Pref. Jour Japan Geotherm Energy Assoc 30:313–335 (in Japanese).

Kurokawa A, Takeo M, Kurita K (2016) Two types of volcanic tremor changed with eruption style during 1986 Izu-Oshima eruption. J Geophys Res Solid Earth 121:2727–2736. https://doi.org/10.1002/2015JB012500.

Maeda Y, Kumagai H, Lacson R, et al (2013) Source process of long-period seismic events at Taal volcano, Philippines: Vapor transportation and condensation in a shallow hydrothermal fissure. J Geophys Res Solid Earth 118:2832–2846. https://doi.org/10.1002/jgrb.50205.

Maeda Y, Kumagai H, Lacson R, et al (2015) A phreatic explosion model inferred from a very long period seismic event at Mayon Volcano, Philippines. J Geophys Res Solid Earth 120:226–242. https://doi.org/10.1002/2014JB011440.

Maeda Y, Kato A, Yamanaka Y (2017) Modeling the dynamics of a phreatic eruption based on a tilt observation: Barrier breakage leading to the 2014 eruption of Mount

Ontake, Japan. J Geophys Res Solid Earth 122:1007–1024.

https://doi.org/10.1002/2016JB013739.

Maeno F, Nakada S, Oikawa T, et al (2016) Reconstruction of a phreatic eruption on 27 September 2014 at Ontake volcano, central Japan, based on proximal pyroclastic density current and fallout deposits the Phreatic Eruption of Mt. Ontake Volcano in 2014 5. Volcanology. Earth Planets Sp 68:82. https://doi.org/10.1186/s40623-016-0449-6.

Mannen K, Yukutake Y, Kikugawa G, et al (2018) Chronology of the 2015 eruption of Hakone volcano, Japan: geological background, mechanism of volcanic unrest and disaster mitigation measures during the crisis. Earth Planets Sp 70:68. https://doi.org/10.1186/s40623-018-0844-2.

Matsunaga Y, Kanda W, Takakura S, et al (2020) Magmatic hydrothermal system inferred from the resistivity structure of Kusatsu-Shirane Volcano. J Volcanol Geotherm

Res 390:106742. https://doi.org/10.1016/j.jvolgeores.2019.106742.

Mayeda K (1991) site amplification from s-wave coda in the long valley caldera region, california. Bull Seismol Soc Am 81:2194–2213.

Mayer K, Scheu B, Gilg HA, et al (2015) Experimental constraints on phreatic eruption processes at Whakaari (White Island volcano). J Volcanol Geotherm Res 302:150–162. https://doi.org/10.1016/j.jvolgeores.2015.06.014.

Mori T, Hirabayashi J, Nogami K, Onizawa S (2006) A new seismic observation system at the Kusatsu-Shirane volcano. Bull Volcanol Soc Japan 53:41–47 (in Japanese with English abstract).

Morioka H, Kumagai H, Maeda T (2017) Theoretical basis of the amplitude source location method for volcano-seismic signals. J Geophys Res Solid Earth 122:6538–6551. https://doi.org/10.1002/2017JB013997.

Motoya Y, Nogushi M (1963) Tremors observed at active volcano, geyser and fumarole. Bull Volcanol Soc Japan 8(1):20–32 (in Japanese with English abstract).

Nakamichi H, Iguchi M, Tameguri T, Sonoda T (2017) Quantification of seismic and acoustic waves to characterize the 2014 and 2015 eruptions of Kuchinoerabujima Volcano, Japan. J Nat Disaster Sci 38:65–83. https://doi.org/10.2328/jnds.38.65.

Nakano M, Kumagai H, Kumazawa M, et al (1998) The excitation and characteristic frequency of the long-period volcanic event: An approach based on an inhomogeneous autoregressive model of a linear dynamic system. J Geophys Res Solid Earth 103(B5):10,031–10,046. https://doi.org/10.1029/98jb00387.

Nakano M, Kumagai H, Chouet BA (2003) Source mechanism of long-period events at Kusatsu-Shirane Volcano, Japan, inferred from waveform inversion of the effective excitation functions. J Volcanol Geotherm Res 122:149–164.

https://doi.org/10.1016/S0377-0273(02)00499-7.

Newhall CG, Self S (1982) The volcanic explosivity index (VEI): an estimate of explosive magnitude for historical volcanism. J Geophys Res 87:123–1238. https://doi.org/10.1029/jc087ic02p01231.

Nigorikawa A, Ishizaki Y, Kametani N, Yoshimoto M, Terada A, Ueki K, Nakamura K (2016) Holocene eruption history of the Motoshirane Pyroclastic Cone Group, Kusatsu-Shirane Volcano. Abstracts of Japan Geoscience Union Meeting 2016 SVC48-11.

Nurhasan, Ogawa Y, Ujihara N, et al (2006) Two electrical conductors beneath Kusatsu-Shirane volcano, Japan, imaged by audiomagnetotellurics, and their implications for the hydrothermal system. Earth Planets Sp 58:1053–1059. https://doi.org/10.1186/BF03352610.

Ogiso M, Yomogida K (2012) Migration of tremor locations before the 2008 eruption of

Meakandake Volcano, Hokkaido, Japan. J Volcanol Geotherm Res 217–218:8–20. https://doi.org/10.1016/j.jvolgeores.2011.12.005.

Ogiso M, Matsubayashi H, Yamamoto T (2015) Descent of tremor source locations before the 2014 phreatic eruption of Ontake volcano, Japan. Earth Planets Sp 67:206. https://doi.org/10.1186/s40623-015-0376-y.

Ohba T, Hirabayashi J, Nogami K (1994) Water, heat and chloride budgets of the crater lake, Yugama at Kusatsu-Shirane volcano, Japan. Geochem Jour 28:217–231.

Ohba T, Hirabayashi J, Nogami K (2000) D/H and 18O/16O ratios of water in the crater lake at Kusatsu-Shirane volcano, Japan. J Volcanol Geotherm Res 97:329–346. https://doi.org/10.1016/S0377-0273(99)00169-9.

Ohba T, Yaguchi M, Kumehara S, Terada A (2016) Volcanic activity of Mt Kusatsu-Shirane suggested by the variations in fumarolic gas composition and crater lake water

chemistry. Abstracts of Japan Geoscience Union Meeting 2016 SVC45-01 (in Japanese).

Ohminato T (2006) Characteristics and source modeling of broadband seismic signals associated with the hydrothermal system at Satsuma-Iwojima volcano, Japan. J Volcanol Geotherm Res 158:467–490. https://doi.org/10.1016/j.jvolgeores.2006.08.004.

Ohwada M, Ohba T, Hirabayashi J, Nogami K, Nakamura K, Nagao K (2003) Interaction between magmatic fluid and meteoric water, inferred from 18O/16O and 36Ar/H2O ratios of fumarolic gases at the Kusatsu Shirane volcano, Japan. Earth Planets Sp 55:105–110. https://doi.org/10.1186/BF03351737.

Ossaka J, Ozawa T, Nomura T, Ossaka T, Hirabayashi J, Takaesu A, Hayashi T (1980) Variation of chemical compositions in volcanic gases and waters at Kusatsu-Shirane volcano and its activity in 1976. Bull Volcanol 43:207– 216.

Phillips WS, Aki K (1986) Site amplification of coda waves from local earthquakes in central California. Bull Seismo Soc Am 76(3):627–648.

Stix J, de Moor JM (2018) Understanding and forecasting phreatic eruptions driven by magmatic degassing. Earth Planets Sp 70:83. https://doi.org/10.1186/s40623-018-0855-z.

Takahashi K, Fujii I (2014) Long-term thermal activity revealed by magnetic measurements at Kusatsu-Shirane volcano, Japan. J Volcanol Geotherm Res 285:180–194. https://doi.org/10.1016/j.jvolgeores.2014.08.014.

Takemura S, Furumura T, Saito T (2009) Distortion of the apparent S-wave radiation pattern in the high-frequency wavefield: Tottori-Ken Seibu, Japan earthquake of 2000. Geophys J Int 178:950–961. doi:10.1111/j.1365-246X.2009.04210.x

Tameguri T, Iguchi M, Nakamichi H, Yamamoto K (2016) Disaster Research of

Kuchinoerabujima Eruptions in 2014–2015. Annuals of Disas Prev Res Inst 59(A) (in Japanese with English abstract).

Tanada T, Ueda H, Nagai M, Ukawa M (2017) NIED's V-net, the fundamental volcano observation network in Japan. J Disaster Res 12:926–931. https://doi.org/10.20965/jdr.2017.p0926.

Terada A, Aoyama H, Nogami K, Yamawaki T, Saito M (2011) A source model of the ground deformation observed during the volcanic tremor on 27 May 2011: An image of a volcanic fluid ascent process inferred from a tiltmeter net- work of Kusatsu-Shirane volcano. Abstracts of the Volcanological Society of Japan 2011 Fall Meeting: A3-01 (in Japanese).

Terada A, Sakamoto Y, Kanda W, Ogawa Y (2016) Mass budgets of hydrothermal water beneath hot crater lakes at Kusatsu-Shirane volcano evaluated by ground deformation and changes in thermal activities. Abstracts of Japan Geoscience Union Meeting 2016

SVC45-05.

Terada A, Hashimoto T (2017) Variety and sustainability of volcanic lakes: Response to subaqueous thermal activity predicted by a numerical model. J Geophys Res Solid Earth 122:6108–6130. https://doi.org/10.1002/2017JB014387.

Terada A (2018) Kusatsu-Shirane volcano as a site of phreatic eruptions. Jour Geol Soc Japan 124(4): 251–270 (in Japanese and English abstract).

The Joint Research Team for ash fall in Kusatsu-Shirane 2018 eruption (2018) Ash fall distribution of Jan. 23, 2018, eruption in Kusatsu-Shirane Volcano. Reports of Coordinating Committee for Prediction of Volcanic Eruption No.129. Jpn Meteorol Agency, Tokyo. https://www.data.jma.go.jp/svd/vois/data/tokyo/STOCK/kaisetsu/CCPVE/Report/129/kaiho_129_10.pdf. Accessed 15 July 2020.

Tseng K H, Ogawa Y, Nurhasan, Tank S B, Ujihara, N, Honkura Y, Terada A, Usui Y, Kanda W, (under review) Anatomy of Active Volcanic Edifice at the Kusatsu-Shirane Volcano, Japan, by Magnetotellurics: Hydrothermal Implications for Volcanic Unrests. Earth Planets Sp.

Ueda H, Nagai M, Tanada T (2018) Phreatic eruptions and deformation of Ioto Island (Iwo-jima), Japan, triggered by deep magma injection. Earth Planets Sp 70:38. https://doi.org/10.1186/s40623-018-0811-y.

Ueki K, Terada A (2012) Field excursion guide to Kusatsu-Shirane volcano. Bull Volcanol Soc Japan 57:235–251 (in Japanese).

Usu Volcano Observatory (1997) The March, 1996 Eruption of Mt. Komagatake, Hokkaido. Reports of Coordinating Committee for Prediction of Volcanic Eruption No.66. Jpn Meteorol Agency, Tokyo. http://www.data.jma.go.jp/svd/vois/data/tokyo/STOCK/kaisetsu/CCPVE/Report/066/k

aiho_066_02.pdf. Accessed 15 July 15 2020.

Uto K, Kurihara A, Hirabayashi J (2004) Core descriptions of seismological observation wells around Shirane cone, Kusatsu Shirane volcano. Report of 4th Joint Observation of Kusatsu-Shirane Volcano 59–68.

Walsh B, Jolly AD, Procter J (2017) Calibrating the amplitude source location (ASL) method by using active seismic sources: An example from Te Maari volcano, Tongariro National Park, New Zealand. Geophys Res Lett 44:3591–3599. https://doi.org/10.1002/2017GL073000.

Walsh B, Procter J, Lokmer I, et al (2019) Geophysical examination of the 27 April 2016 Whakaari/White Island, New Zealand, eruption and its implications for vent physiognomies and eruptive dynamics. Earth, Planets Sp 71:25. https://doi.org/10.1186/s40623-019-1003-0.

Yamamoto M, Aoyama H, Tsutsui T, Terada A, Kanada W, Ogawa W (2018) Temporary seismic observation at Kusatsu-Shirane volcano, Japan. Abstracts of Japan Geoscience Union Meeting 2018 SVC41-P10.

Yukutake Y, Honda R, Harada M, et al (2017) Analyzing the continuous volcanic tremors detected during the 2015 phreatic eruption of the Hakone volcano. Earth Planets Sp 69:164. https://doi.org/10.1186/s40623-017-0751-y.

Yukutake Y, Ichihara M, Honda R (2018) Infrasonic wave accompanying a crack opening during the 2015 Hakone eruption. Earth Planets Sp 70:53. https://doi.org/10.1186/s40623-018-0820-x.

Figure Legends

Fig. 1 **a** Location of Kusatsu-Shirane volcano. Black triangles denote active volcanoes

defined by JMA. **b** Locations of V-net stations at Kusatsu-Shirane. Pink diamonds correspond to major thermal spring sites. A black square is the map area of **c**. **c** A detailed map including Yugama, Ainomine, and Motoshirane. Blue and white squares show observation stations operated by KSVO and JMA. Vent locations of the 2018 eruption and unidentified past events are denoted by red and violet colors (GSI, 2018). Seismic data at stations of YNE and KSJ are adopted in hypocenter determinations by KSVO, although we do not adopt ASL analysis in this paper.

Fig. 2 **a** Horizontal and vertical-NS cross-sections of hypocenters of volcanic earthquakes determined by KSVO. Vent locations of the 2018 eruptions are represented by red color. A black star shows a reference point for infrasound waveform plot in Fig. 5 and ASL analysis. **b** A time series of seismicity at Kusatsu-Shirane in the period from June 2016 to December 2018.

Fig. 3 **a** Raw vertical ground velocity waveform at KSW from 09:58 on 23 January 2018. **b** Filtered (Gray: 0.5–5 Hz; Red: 5–20 Hz) vertical ground velocity waveforms at KSW. **c**

Tilt change records at KSHV. An acausal low-pass filter with a cut-off frequency of 0.05 Hz is applied to emphasize dynamic tilt changes. The cumulative squared amplitude of filtered vertical ground velocity at KSW is also shown to compare tilt changes and excitation of the 5–20 Hz band seismic signals. **d** Raw infrasound waveform at KSRH.

Fig. 4 **a** Fourier spectra for the vertical ground velocity at KSW (Red: for 500 s from 09:58:19; Green: for 100 s from 10:14:09; Gray: for 500 s from 09:50:00). Pink color corresponds to the frequency band of 5–20 Hz, which is focused on our ASL analysis. **b** Spectrum ratios to background signals.

Fig. 5 Infrasound records at KSRH and KSAO. The vertical offset of each waveform denotes horizontal distances from the center of active vents of the 2018 eruption denoted in Fig. 2a. An apparent propagation velocity (V_i) of 340 m/s is also shown by a red line.

Fig. 6 **a** Values of RES with different source elevations beneath the crater setting S_i

as 1. **b** Modeled amplitude at an elevation of 2050 m (the ground surface) for the reference time window. Red bars correspond values of S_i at each station.

Fig. 7 **a** Horizontal locations of estimated tremor sources. The color of each plot corresponds to a contour bar in **b**. Epicenters of volcanic earthquakes in Fig. 2 are also shown by gray dots. A plot with a green square is the fixed source location for the reference time window. **b** Analyzed filtered (5–20 Hz) vertical ground velocity at KSW, estimated source elevations, and the minimum RES value of each time window.

Fig. 8 Spatial distributions of RES values in three cross-sections through the point (star) with the minimum RES value for a time window of 120 s in Fig. 7. Red plots represent vent locations of the 2018 eruptions.

Fig. 9 Schematic illustration of interpretation for examined volcanic tremor in the 2018 eruption and related hydrothermal system structure at Kusatsu-Shirane volcano. Hydrothermal fluid ascends (gray broken arrows) beneath Shirane and Ainomine

induces surrounding seismic activity. A red arrow corresponds inferred hydrothermal fluid injection to the cap-rock layer and that induced volcanic tremor.

Table Legends

Table 1 Instruments details of seismic networks at Kusatsu-Shirane volcano.

	Station	Sensor	Natural period / Flat response	Sampling	Data logger / Resolution
Short period seismometer	KSE, KSS, and KSW (KSVO)	JTS-33 (Akashi)	1 s	200 Hz	LS-7000XT (Hakusan) / 22 bit
	KSYG and JIE (KSVO)	L4 (Mark Product)	1 s	200 Hz	LS-7000XT (Hakusan) / 22 bit
	KSHV, KSNV, and KSYV (NIED)	JTS-33 (Mitsutoyo)	1 s	100 Hz	HKS-9200/9300 (Keisokugiken) / 27 bit
	KSAO (JMA)	JTS-23	1 s	100 Hz	S502G (Meisei) / 24

		(Mitsutoyo)			bit
	KSHA (JMA)	L4-C (Mark Product)	1 s	100 Hz	LS-7000XT (Hakusan) / 24 bit
Infrasound microphone	KSRH (KSVO)	SI-102 (Hakusan)	0.05–100 Hz	200 Hz	LS-7000XT (Hakusan) / 22 bit
	KSAO (JMA)	ACO 3348 (Aco)	0.1–100 Hz	100 Hz	TYPE 7144 (Aco) / 16 bit
Tiltmeter	KSHV, KSNV, and KSYV (NIED)	JTS-33 (Mitsutoyo)	DC–5 Hz	20 Hz	HKS-9200/9300 (Keisokugiken) / 27 bit

Figures

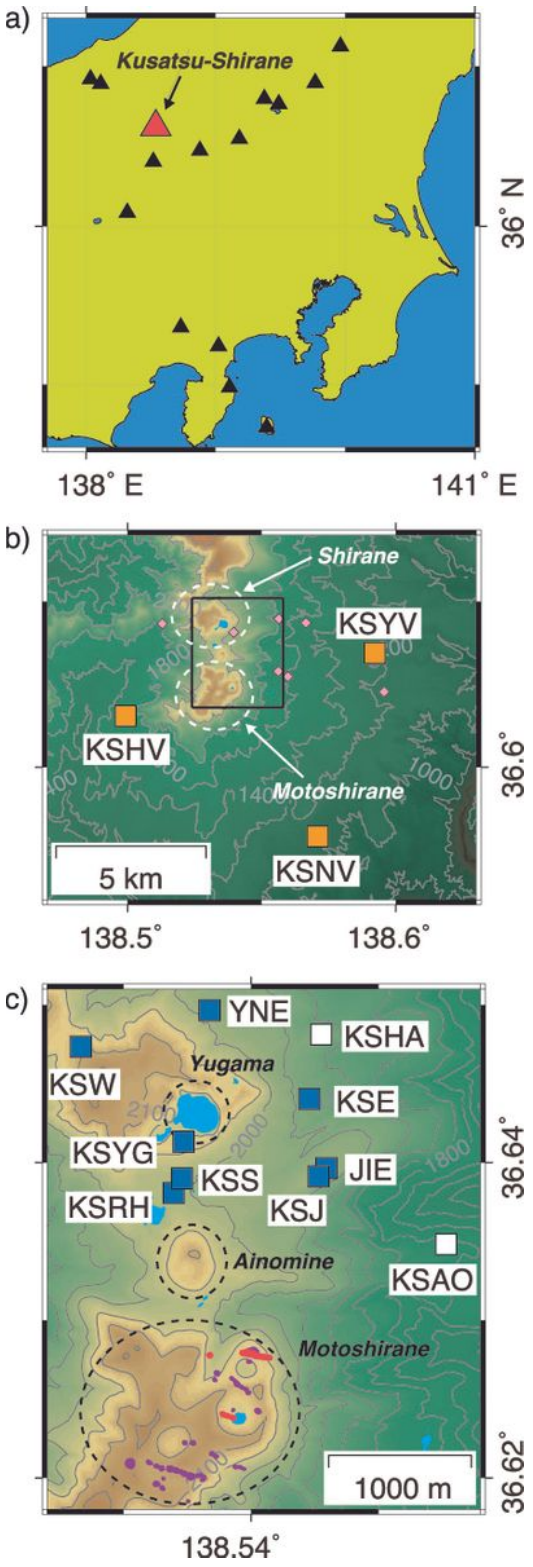

Figure 1

a Location of Kusatsu-Shirane volcano. Black triangles denote active volcanoes defined by JMA. b Locations of V-net stations at Kusatsu-Shirane. Pink diamonds correspond to major thermal spring sites. A black square is the map area of c. c A detailed map including Yugama, Ainomine, and Motoshirane.

Blue and white squares show observation stations operated by KSVO and JMA. Vent locations of the 2018 eruption and unidentified past events are denoted by red and violet colors (GSI, 2018). Seismic data at stations of YNE and KSJ are adopted in hypocenter determinations by KSVO, although we do not adopt ASL analysis in this paper.

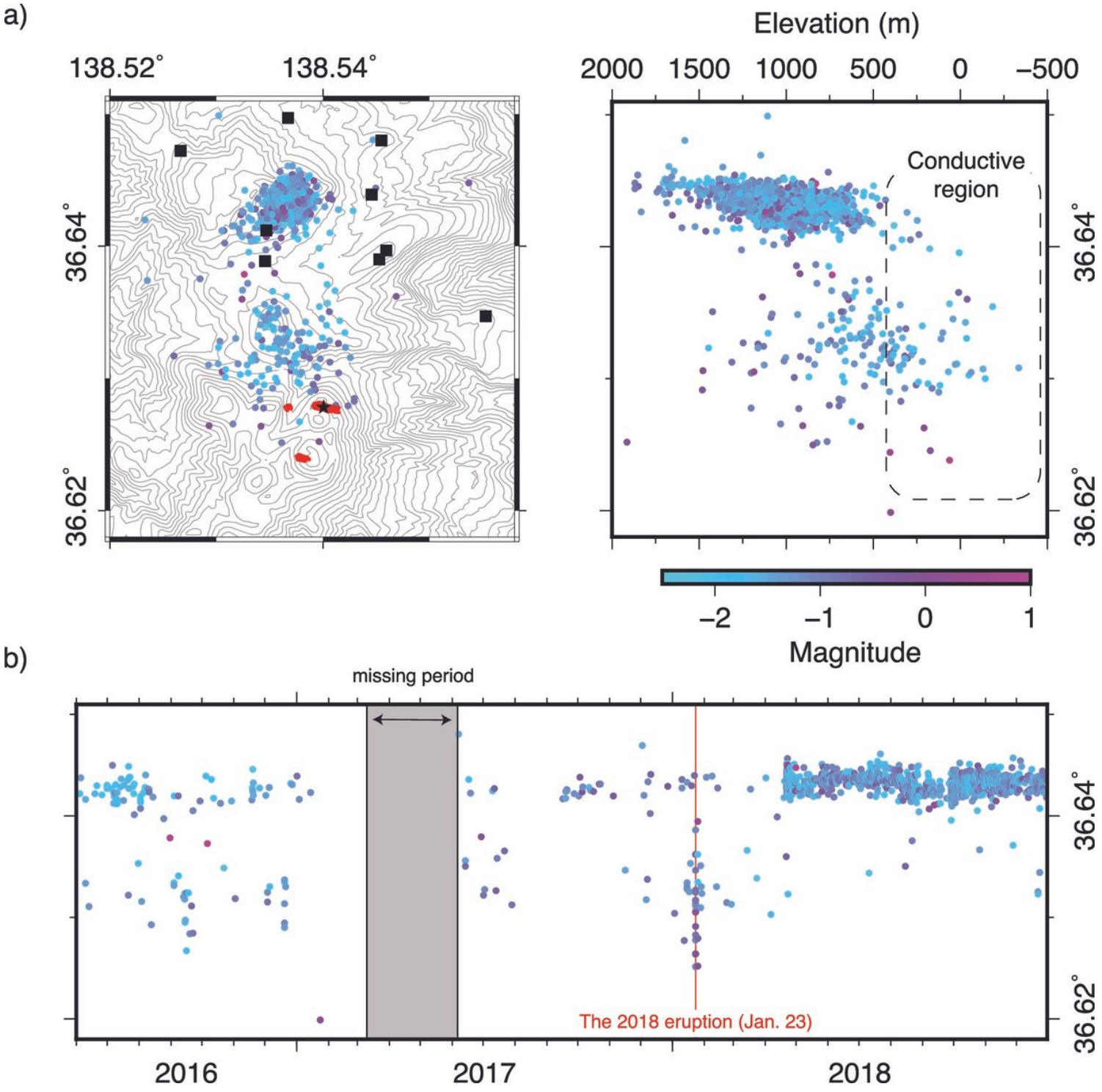

Figure 2

a Horizontal and vertical-NS cross-sections of hypocenters of volcanic earthquakes determined by KSVO. Vent locations of the 2018 eruptions are represented by red color. A black star shows a reference point for

infrasound waveform plot in Fig. 5 and ASL analysis. b A time series of seismicity at Kusatsu-Shirane in the period from June 2016 to December 2018.

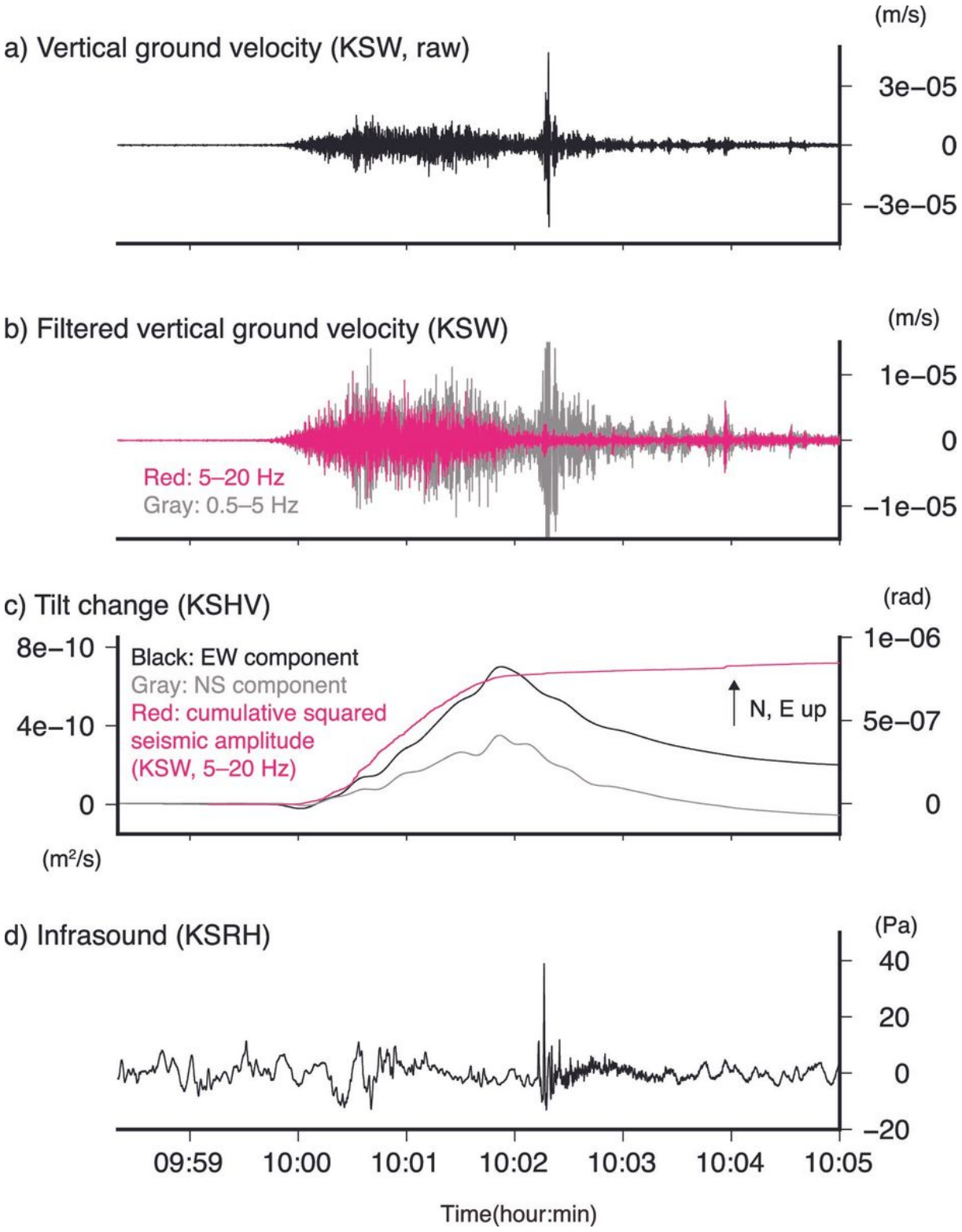

Figure 3

a Raw vertical ground velocity waveform at KSW from 09:58 on 23 January 2018. b Filtered (Gray: 0.5–5 Hz; Red: 5–20 Hz) vertical ground velocity waveforms at KSW. c Tilt change records at KSHV. An acausal low-pass filter with a cut-off frequency of 0.05 Hz is applied to emphasize dynamic tilt changes. The

cumulative squared amplitude of filtered vertical ground velocity at KSW is also shown to compare tilt changes and excitation of the 5–20 Hz band seismic signals. d Raw infrasound waveform at KSRH.

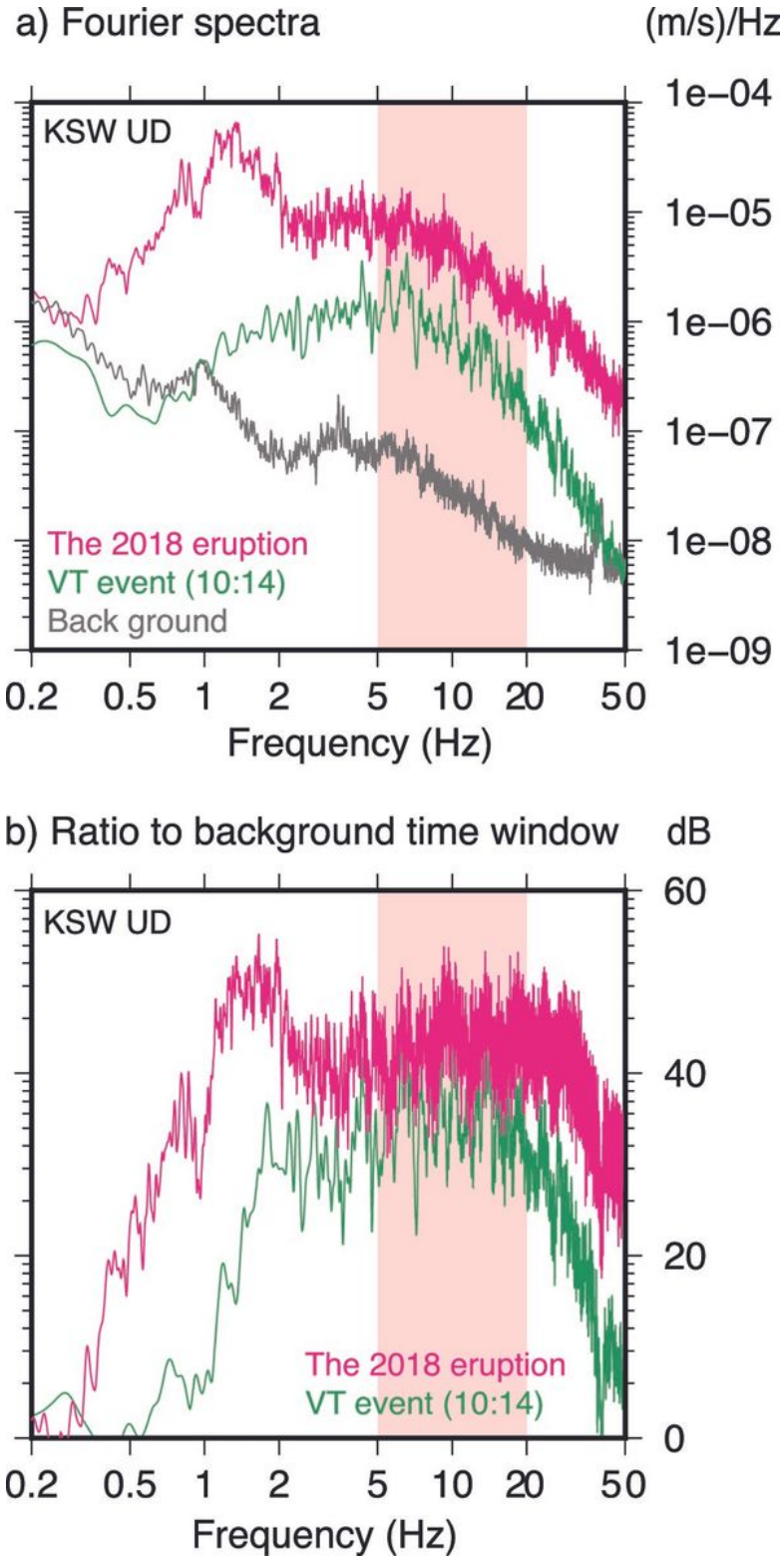

Figure 4

a Fourier spectra for the vertical ground velocity at KSW (Red: for 500 s from 09:58:19; Green: for 100 s from 10:14:09; Gray: for 500 s from 09:50:00). Pink color corresponds to the frequency band of 5–20 Hz, which is focused on our ASL analysis. b Spectrum ratios to background signals.

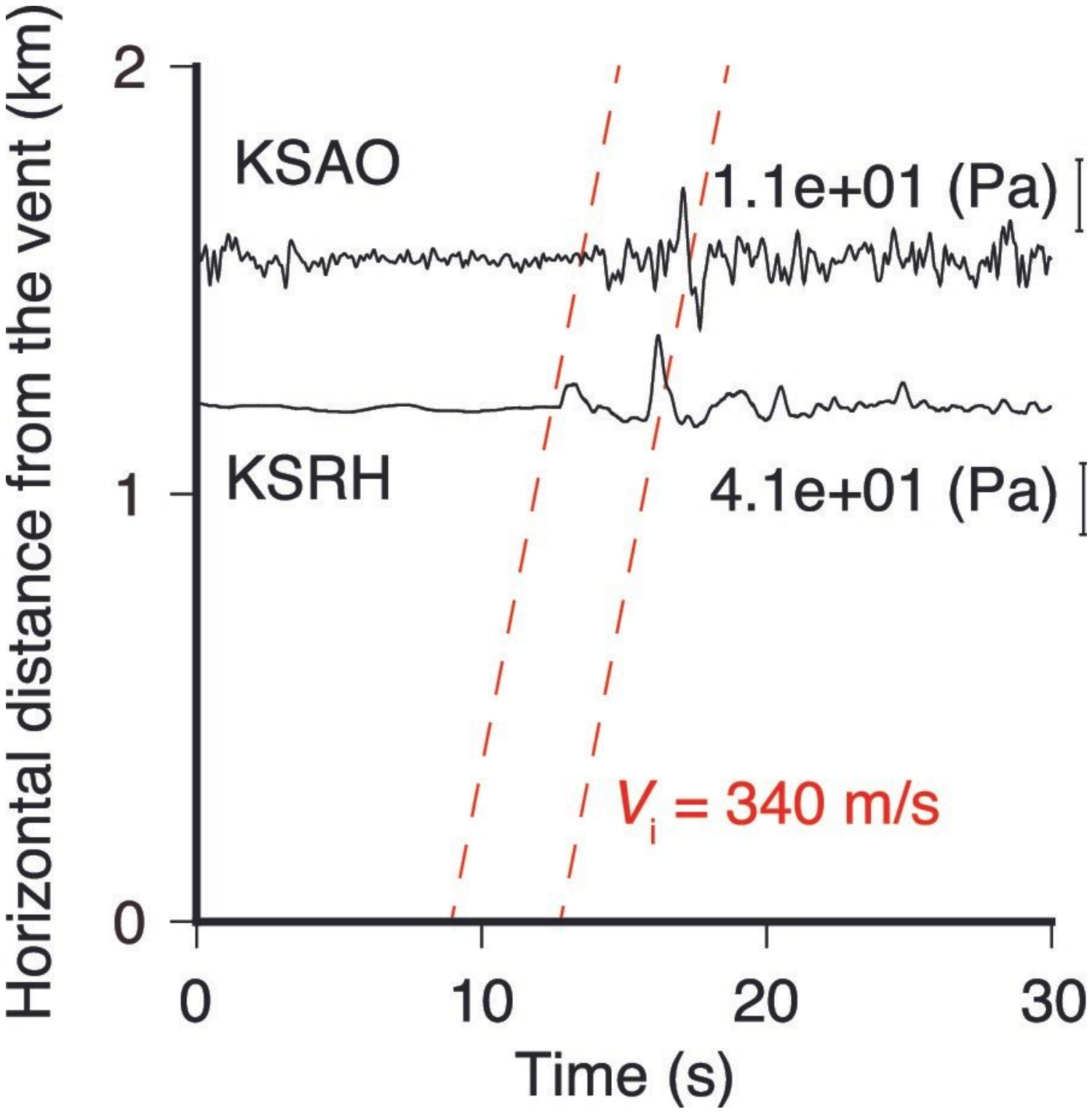

Figure 5

Infrasound records at KSRH and KSAO. The vertical offset of each waveform denotes horizontal distances from the center of active vents of the 2018 eruption denoted in Fig. 2a. An apparent propagation velocity (V_i) of 340 m/s is also shown by a red line.

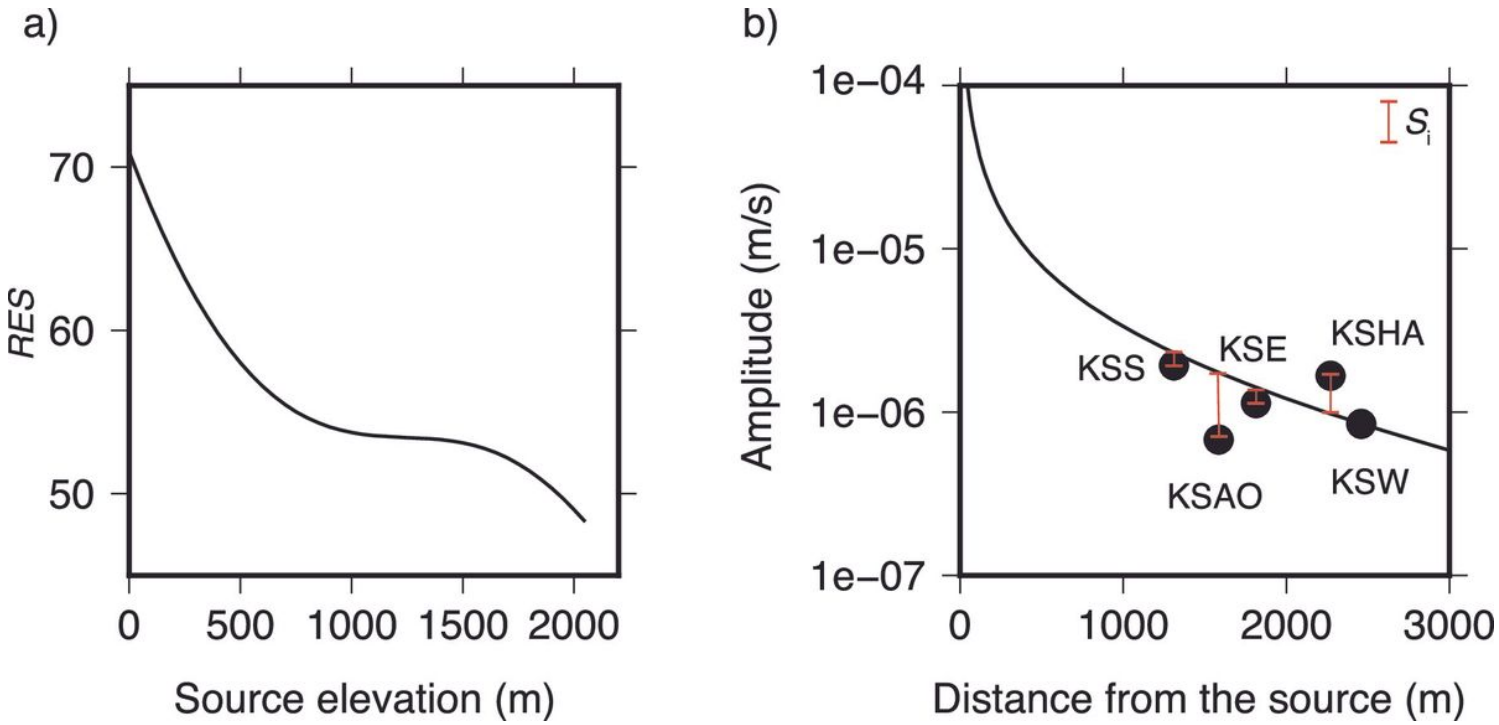

Figure 6

a Values of RES with different source elevations beneath the crater setting S_i as 1. b Modeled amplitude at an elevation of 2050 m (the ground surface) for the reference time window. Red bars correspond values of S_i at each station.

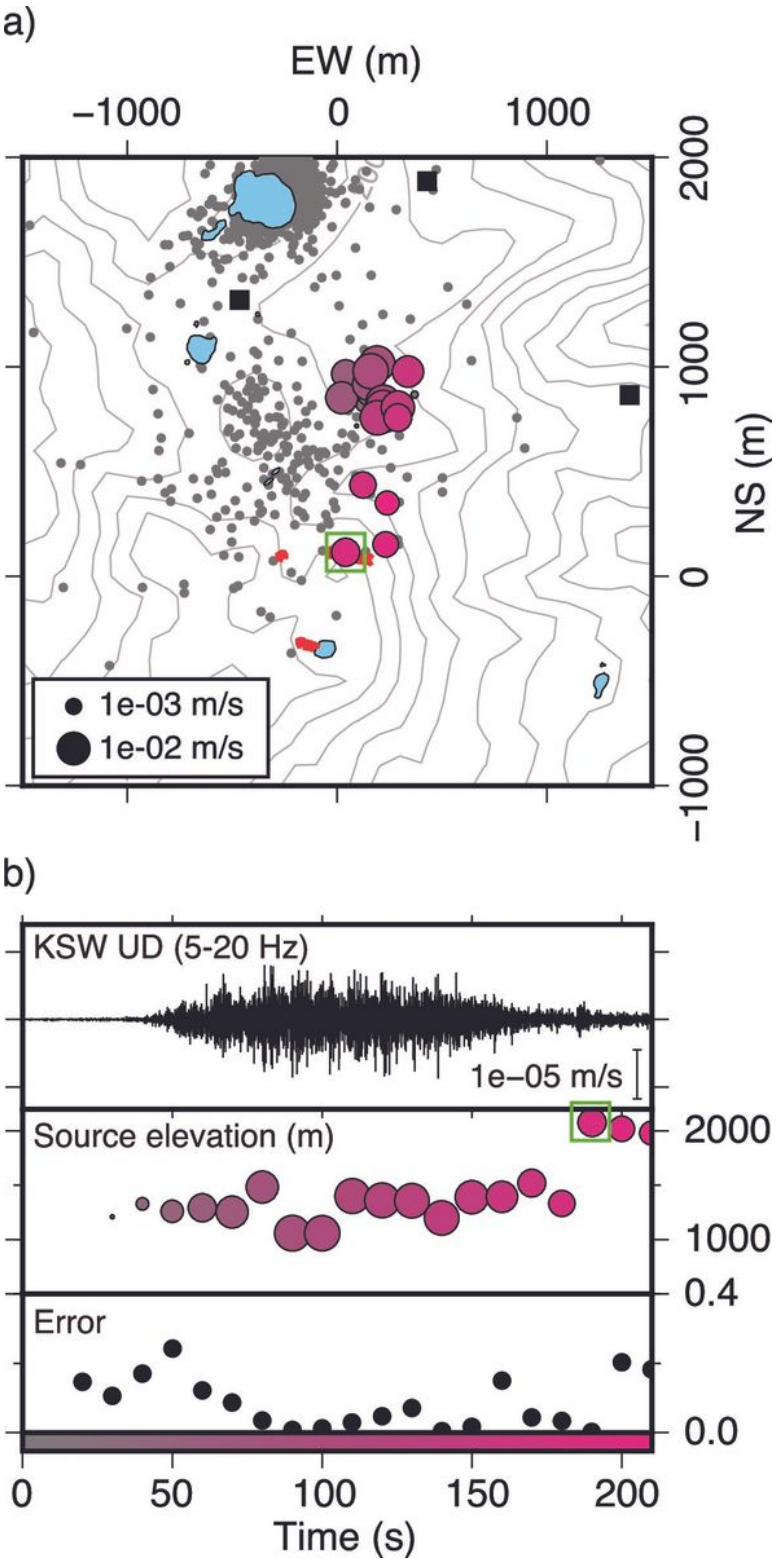

Figure 7

a Horizontal locations of estimated tremor sources. The color of each plot corresponds to a contour bar in b. Epicenters of volcanic earthquakes in Fig. 2 are also shown by gray dots. A plot with a green square is the fixed source location for the reference time window. b Analyzed filtered (5–20 Hz) vertical ground velocity at KSW, estimated source elevations, and the minimum RES value of each time window.

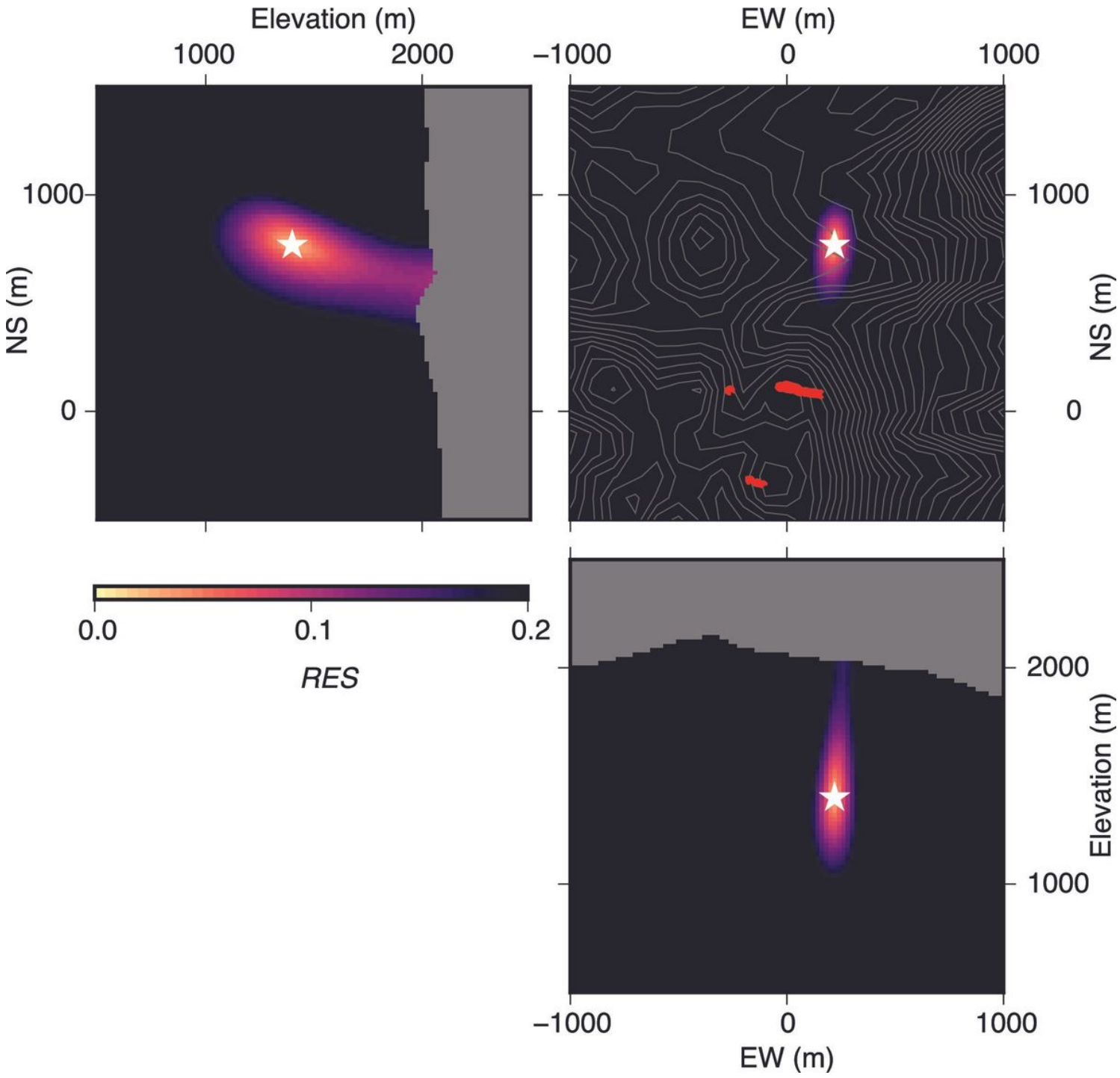

Figure 8

Spatial distributions of RES values in three cross-sections through the point (star) with the minimum RES value for a time window of 120 s in Fig. 7. Red plots represent vent locations of the 2018 eruptions.

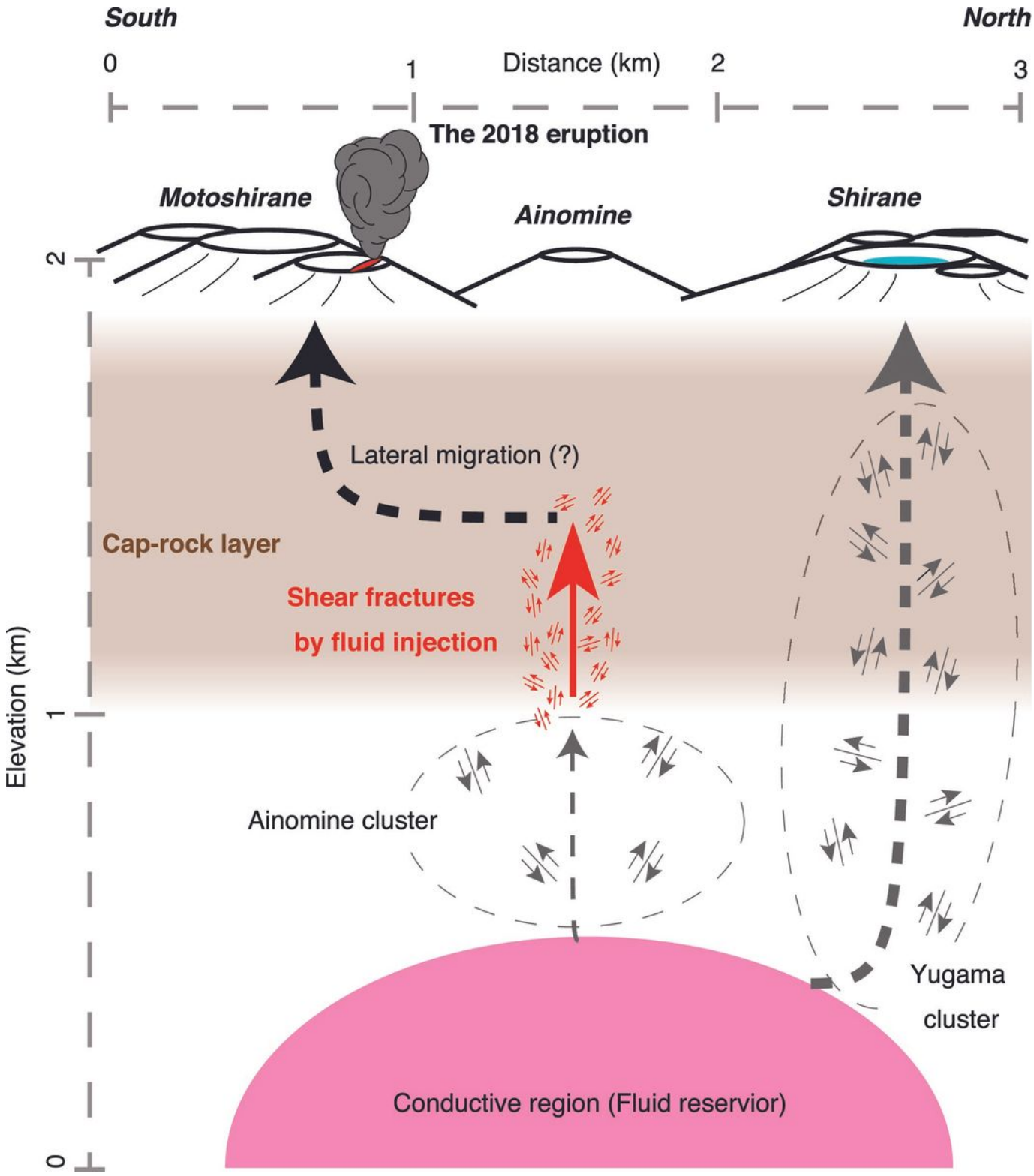

Figure 9

Schematic illustration of interpretation for examined volcanic tremor in the 2018 eruption and related hydrothermal system structure at Kusatsu-Shirane volcano. Hydrothermal fluid ascends (gray broken arrows) beneath Shirane and Ainomine induces surrounding seismic activity. A red arrow corresponds inferred hydrothermal fluid injection to the cap-rock layer and that induced volcanic tremor.

Supplementary Files

This is a list of supplementary files associated with this preprint. Click to download.

- 20200903.png
- AdditionalFIle120200909.docx
- AdditionalFIle220200909.docx